Regular Article

PHYSICAL CHEMISTRY RESEARCH
Published by the
Iranian Chemical Society
www.physchemres.org
info@physchemres.org

Phys. Chem. Res., Vol. 10, No. 4, 473-483, December 2022
DOI: 10.22036/PCR.2022.313916.1980

Spherical α-Fe_2O_3 Nanoparticles: Synthesis and Characterization and Its Photocatalytic Degradation of Methyl Orange and Methylene Blue

A.D. Khalaji*

Department of Chemistry, Faculty of Science, Golestan University, Gorgan, Iran

(Received 29 November 2021, Accepted 2 February 2022)

The spherical iron oxide (α-Fe_2O_3) nanoparticles were prepared using facile, low-cost and environmental friendly one step thermal decomposition of $Fe(NO_3)_3{\cdot}3H_2O$ at the presence of malic acid (mass ration 1:1) at 600 °C for 3 h. The product was characterized by Fourier transform infrared (FT-IR) spectroscopy, powder X-ray diffraction (XRD), vibrating sample magnetometer (VSM), and transmission electron microscope (TEM). The FT-IR and XRD results predicted the formation of single phase of rhombohedral α-Fe_2O_3 nanoparticles. TEM image illustrated that the α-Fe_2O_3 nanoparticles had spherical shapes. VSM result showed that the as-prepared α-Fe_2O_3 nanoparticles were ferromagnetic materials with M_s of 1.96 emu g^{-1}. The photocatalytic activity of the α-Fe_2O_3 nanoparticles was evaluated by the photodegradation of methyl orange (MO) and methyl blue (MB) in aqueous solution under visible light irradiation. The effects of pH solution, sorbent dose, contact time (0-120 min), and initial concentration of dyes (30, 50 and 70 mg l^{-1}) were also studied. At the end of the process, the catalyst could be separated and recovered using an external magnetic field. The results indicate that the α-Fe_2O_3 nanoparticles can be used as an efficient photocatalyst for removal of other dyes from aqueous solution, and has benefits for large-scale production.

Keywords: α-Fe_2O_3 nanoparticles, Decomposition, Methyl orange, Methyl blue, Photocatalyst

INTRODUCTION

Transition metal oxides and ferrites such as NiO [1], Co_3O_4 [2], CuO [3], Mn_2O_3 [4], Mn_3O_4 [5], CeO_2 [6,7], $Ni_xCo_{(0.5-x)}Zn_{0.5}Fe_2O_4$ [8], $NiFe_2O_4$ [9], and Fe_2O_3 [10-12] have vast applications in Li-ion batteries, photocatalytic degradation and removal of organic dyes, supercapacitor, optical materials, antibacterial materials, and removal of heavy metal ions. Recently, environmental pollution, in particular water contamination, is one of the major problems facing human society [1-3]. Subsequently, removal of organic dye pollutions from wastewater using adsorption [13] and photocatalytic degradation reaction [14-16] is important due to its economic and environmental benefits. So far, various metal oxides as catalyst have been used to remove various contaminants from the wastewaters or aqueous solutions [2,3-14-16]. Among them, hematite iron oxide (α-Fe_2O_3) nanoparticles, with corundum structure, is widely used for photocatalytic removal of various organic dyes such as bisphenol A [14], rhodamine B [17] methyl orange [18], and Congo red [16]. The α-Fe_2O_3 is very stable, the oldest known iron oxide, and the end form of transformations of iron oxides [18]. Until now, various morphologies of α-Fe_2O_3 nanoparticles with different crystalline structure were used for photocatalytic degradation of organic dyes [14-18]. The physical and chemical properties of α-Fe_2O_3 nanoparticles can be tuned by controlling their size, shape, and the synthesis parameters [14-18]. Recently, spherical α-Fe_2O_3 nanoparticles were synthesized using different techniques; they have application in different fields [19-22]. Ye *et al.* [14] reported the rhombohedral α-Fe_2O_3 as an efficient photocatalytic degradation (about 91%) of bisphenol A. Wang *et al.* [18] studied the mesoporous magnetic Fe_2O_3 nanoparticles as catalyst under visible light irradiation to remove methyl orange from wastewater. The α-Fe_2O_3, with

*Corresponding author. E-mail: alidkhalaji@yahoo.com

a narrow band gap of 2.1 eV [18], is a well candidate for being used in photocatalytic degradation of organic dyes, due to adsorption of visible light from the solar energy [14-18]. Therefore, photocatalytic degradation reaction of organic dyes is economical, ecofriendly, which causes to save fossil fuel [14-18].

Azo dyes such as MO and MB are widely used in various industries such as textile, paper printing, leather and clothes. About 15% of the dyes are discharged into the environment, mainly in water supply [9]. They are very stable, toxic, and hazardous. High concentration of them leads to severe health issues for human such as tumors, skin irritation, mutations, and allergies [23]. So, the degradation of these organic dyes using photocatalytic process has been gained great attention in recent years [24-30]. Photocatalytic transformation process is known as a favorable procedure for preparation of valuable compounds [31-33]. Recently, advanced oxidation processes (AOPs), as an emerging technology, gained great attention for application in many wastewater treatments [34-38]; it produces strong oxidizing agent such as hydroxyl radicals to oxidize the organic compounds. Hydroxyl radicals can be produced by ultraviolet/visible light irradiation [37-38]. Also, the quantum calculations using density functional theory (DFT) was used to confirm the adsorption mechanism of different pollutions on the various adsorbents [39-42].

Continuing the previous work on the preparation of various transition metal nanoparticles [43-47], in this work, hematite (α-Fe_2O_3) nanoparticles were prepared and characterized by low-cost and environmental friendly one step thermal decomposition. In addition, photocatalytic degradation of MO and MB under visible light irradiation using as-prepared α-Fe_2O_3 nanoparticles was studied.

EXPERIMENTAL

Materials and Methods

Ferric nitrate three hydrate, used as a source of Fe, malic acid, methyl orange, and methyl blue dyes were purchased from Merck Company. FT-IR spectrum was recorded with a Perkin-Elmer spectrum from 4000 to 400 cm^{-1}. The XRD pattern was recorded by Netherlands X'Pert PRO diffractometer with a Cu-Kα source from 20-70°. TEM images were obtained by JEOL 2100 UHR-TEM microscope. A 300 W xenon lamp with a 420 nm cutoff filter was use as visible light irradiation source. The magnetic properties of the as-synthesized α-Fe_2O_3 nanoparticles were recorded using vibration sample magnetometer (VSM). UV-Vis spectrum was done using a UV-Vis Perkin-Elmer spectrophotometer in the wavelength ranges of 250-850 nm at room temperature. The specific surface area and pore size distribution of as-prepared α-Fe_2O_3 nanoparticles were calculated by the Brunauer-Emmett-Teller (BET) method and Barrett-Joyner-Halenda (BJH) model, respectively.

Preparation of the α-Fe_2O_3 Nanoparticles

3 g of ferric nitrate three hydrate and 3 g malic acid were vigorously mixed for 10 min in a crucible to obtain a uniform pale-brown powder. The obtained mixture calcined at 600 °C for 3 h in the electrical furnace at air atmosphere. The resulting black precipitates were washed several times with cold distilled water, filtered off and dried. The products characterized by FT-IR, XRD, VSM, and TEM.

Evaluation of Photocatalytic Activity

Various amount (0.02 g) of α-Fe_2O_3 nanoparticles as adsorbent was added to a 50 ml of 30, 50, and 70 mg l^{-1} MO and/or MB aqueous solution, and sonicated for 1 h in the dark to achieved adsorption-desorption equilibrium. After visible light irradiation for various time (0-120 min), 5 ml of solution was collected, centrifuged to separated catalyst, and then the solution absorbance was measured using UV-Vis spectrophotometer.

RESULTS AND DISCUSSION

Characterization of α-Fe_2O_3 Nanoparticles

The FT-IR spectrum of α-Fe_2O_3 nanoparticles (Fig. 1) was recorded using KBr pellet from 400 to 4000 cm^{-1}. As seen in Fig. 1, the sharp peak at about 553 cm^{-1} is assigned to the stretching vibration of F-O, and the peak at 467 cm^{-1} is assigned to the bending vibration of O-Fe-O [13,16].

Figure 2 shows the X-ray diffraction patterns of the as-prepared hematite (α-Fe_2O_3) nanoparticles at 600 °C for 3 h. The characteristic diffraction peaks appeared at 2θ = 24.19 (012), 33.17 (104), 35.68 (110), 40.94 (113), 49.54 (024), 54.19 (116), 57.59 (018), 62.47 (1010), and 64.02 (220)

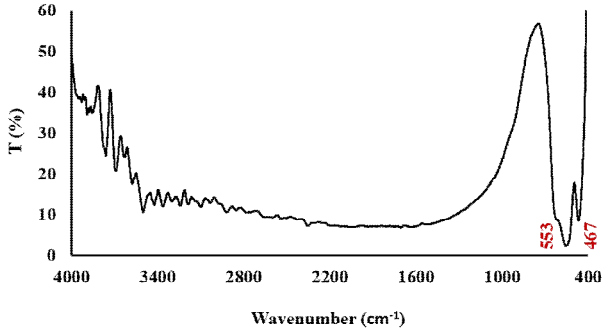

Fig. 1. FT-IR spectrum of the as-prepared α-Fe_2O_3 Nanoparticles.

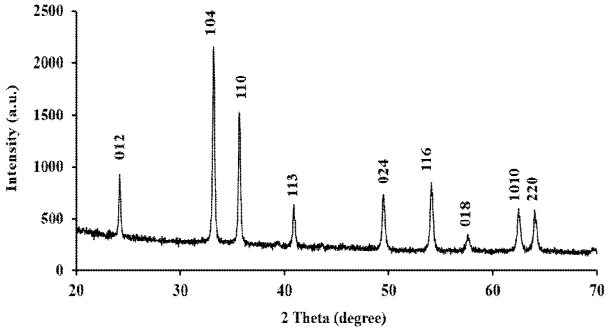

Fig. 2. XRD pattern of the as-prepared α-Fe_2O_3 Nanoparticles.

were confirmed the pure rhombohedral alpha phase of iron oxide (α-Fe_2O_3) (JCPDS no. 33-0664) [14,18] with unit cell parameters of a = 5.036 Å, b = 5.036 Å and c = 13.749 Å [48].

The average crystalline size of 34.55 nm was calculated for the as-prepared α-Fe_2O_3 nanoparticles from the two peaks of 104 and 110, and according to Scheerrer equation [14-18], which is consistent with the TEM images (Fig. 3).

$$D = 0.9\,\lambda/\beta\cos\theta \quad (1)$$

In Equation (1), D is the crystallite size (nm), λ is the X-ray wavelength Cu-Kα (0.154 nm), β is the FWHM of the sharp peak, and θ is the angle [14-18].

The TEM image (Fig. 3) shows that the morphology of the as-prepared α-Fe_2O_3 nanoparticles was uniform quasi-spherical shape. The surfaces of the particles were smooth,

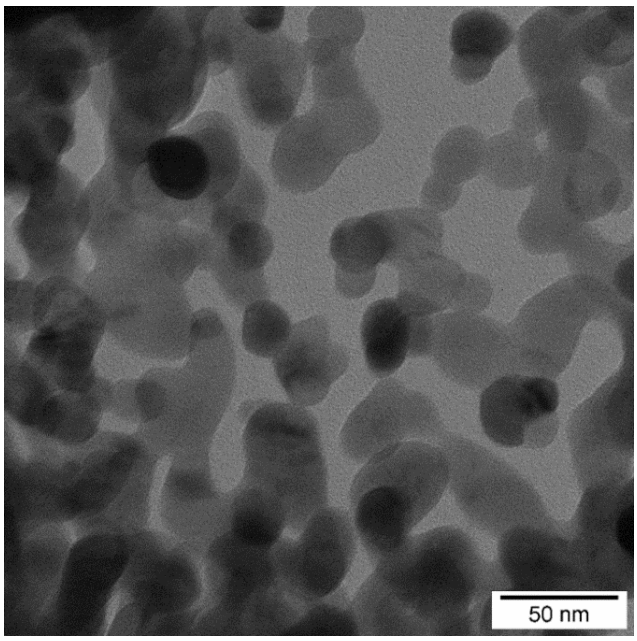

Fig. 3. TEM image of the as-prepared α-Fe_2O_3 nanoparticles.

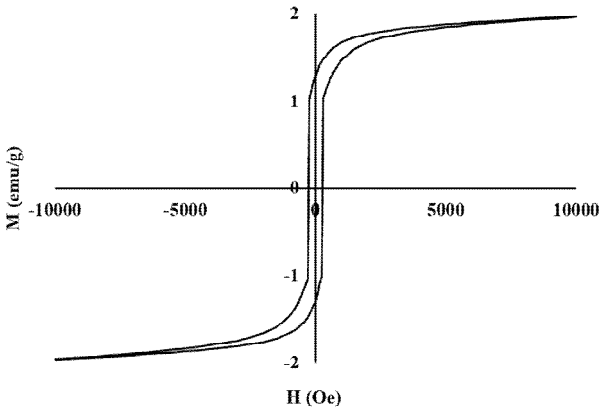

Fig. 4. Magnetic hysteresis loop of the as-prepared α-Fe_2O_3 Nanoparticles.

and the average particle size was less than 50 nm.

M-H curve of the as-prepared α-Fe_2O_3 nanoparticles is shown in Fig. 4, which exhibits the ferromagnetic behavior [49,50]. The saturation (M_s) and remnant (M_r) magnetization were 1.96 and 1.28 emu g^{-1}, while coercivity (H_c) was 275 Oe, known as soft materials. The M_s of the as-prepared α-Fe_2O_3 nanoparticles was lower than that of

spherical α-Fe_2O_3 nanoparticles (6.42 emu g^{-1}) reported by Lassoued *et al.* [49], and higher than that of quasi-cube α-Fe_2O_3 nanoparticles (0.43 emu g^{-1}) for reported by Liu *et al.* [50]. The magnetization saturation value depends on the different structures of α-Fe_2O_3 nanoparticles [49,50].

The UV-Vis absorption was done at room temperature (Fig. 5). There was a peak at 582 nm similar to that reported by Han *et al.* [51] and Khalaji *et al.* [52]. The corresponding band gap energy (E_g), calculated using Equation 2 [53], was found to be 2.13 eV.

$$E_g = 1240/\lambda_{max} \quad (2)$$

In above formulation, λ_{max} is the characteristic UV-Vis peak of the as-prepared α-Fe_2O_3 nanoparticles. So, the as-prepared α-Fe_2O_3 nanoparticles, with narrow band-gap of 2.13 eV [18], can absorb the visible and UV regions of the sunlight and act as a good catalyst for degradation of various organic dyes [14-18].

The surface area and the pore size distribution of as-prepared α-Fe_2O_3 nanoparticles were recorded using nitrogen adsorption-desorption (Fig. 6), indicating that as-prepared α-Fe_2O_3 nanoparticles are mesoporous materials that show typical IUPAC type-IV N_2 adsorption isotherm with H3 type hysteresis loop in high pressure [10,12,14,18]. The calculated BET surface area was 31.278 m^2 g^{-1} [10,12, 14,18].

Photocatalytic Evaluations

In this work, photocatalytic degradation of MO and MB under visible light was investigated. As reported in literature, the OH° and $O_2^{-\circ}$ radicals were generated using α-Fe_2O_3 nanoparticles under UV or visible irradiation [14-18]; they were mainly responsible for the degradation of organic dyes [3]. UV-Vis characteristic peak of MO and MB occurs at 464 and 664 nm [3], respectively; it decreased gradually as the contact time increased.

One of the important parameters that affect the efficiency of photocatalytic degradation of organic dyes is the pH of solution [54-60]. The removal efficiency of as-synthesized α-Fe_2O_3 was carried out under different pH solution from 2-12 using 0.02 g of catalyst. The results are shown in Fig. 7.

The pH solution was adjusted with addition of HCl and

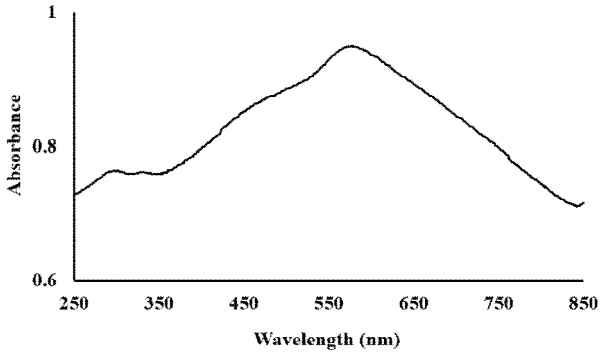

Fig. 5. UV-Vis spectrum of the as-prepared α-Fe_2O_3 Nanoparticles.

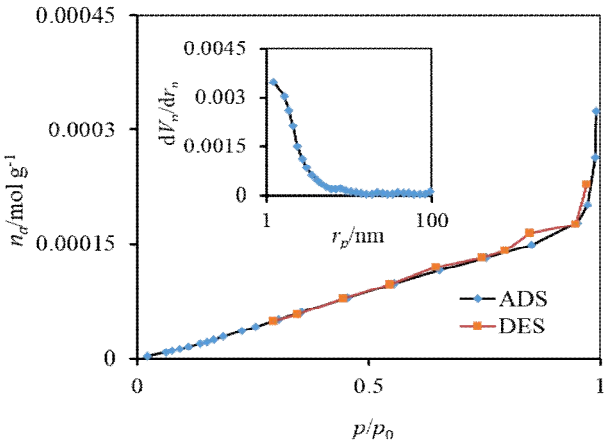

Fig. 6. BET and BJH isotherms of the as-prepared α-Fe_2O_3 Nanoparticles.

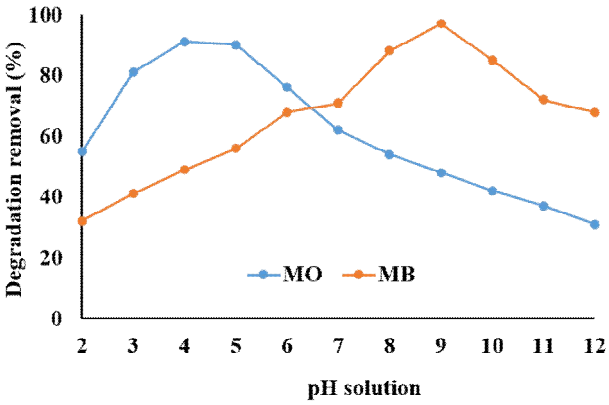

Fig. 7. Effect of pH solution on degradation removal of MO and MB dyes.

NaOH solution (0.1 M). As shown in Fig. 7, the best pHs to achieve high efficiency for photodegradation of MO and MB were 4 and 9, respectively; these are selected for the study of the other parameters. Methyl orange is an anionic dye, while methylene blue is a cationic dye. Hence, the electrostatic interactions of the MO and MB with the surface of the catalyst are contrary to each other. At low pH, the surface of the catalyst was positively charged, and significant electrostatic interaction with the negatively charged MO was obtained [61]. Significant electrostatic interaction between the positively charged MB and the negatively charged surface of the catalyst occurred at high pH [28].

Another effective parameter in photocatalytic degradation of organic dyes is the effect of the amount of catalyst [2,3,7-9,14-18,54-61]. The effect of different doses of catalyst (0.005, 0.01 and 0.02) on the photodegradation of MO and MB was. As shown in Fig. 8, the maximum of photodegradation of dyes occurred when 0.02 g of catalyst was used; this is due to the possibility of producing more h^{+}_{VB} and e^{-}_{CB} to produce oxygen ($O2^{-\circ}$) and hydroxide (OH°) radicals [6,9,8,24-26,30].

Figure 9 shows the degradation profiles of MO and MB (30 mg l^{-1}) under visible light irradiation at various times in presence of 0.02 g α-Fe_2O_3. After 70 min of exposure to visible light, 97% degradation of MB took place that is faster than degradation of MO (90 min, 91%) [15]. Table 1 show the time for degradation of MO and MB over the various catalysts.

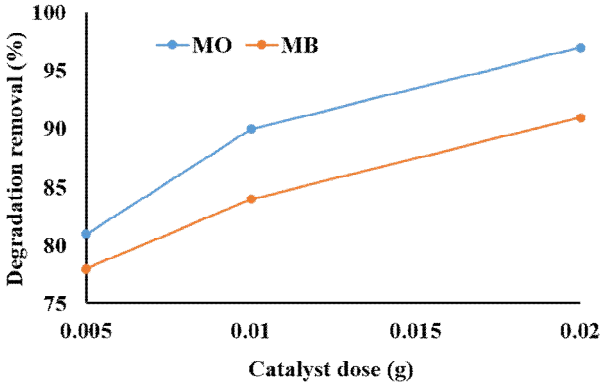

Fig. 8. Effect of catalyst dose on degradation removal of MO and MB dyes.

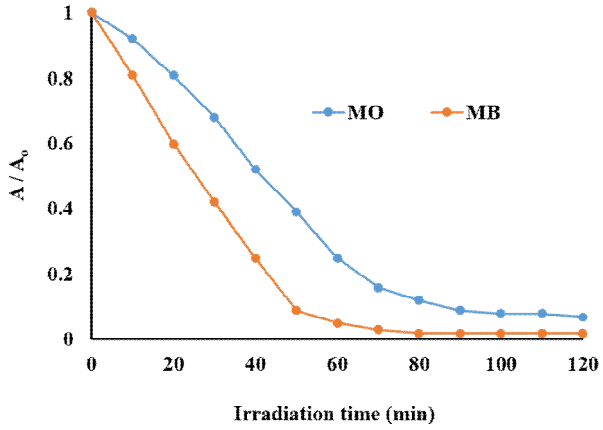

Fig. 9. Comparison of the degradation efficiency for the MO and MB dyes.

Table 1. Photocatalytic Activity of Various Catalysts for Degradation of MO and MB

Photocatalyst	Degradation time (min)	Degradation rate (%)	Dye	Ref.
TiO_2/ZnO	30	97	MO	[30]
CeO_2	60	98	MB	[26]
Pristine CeO_2	175	100	MB	[24]
CeO_2	75	85	MB	[6]
Fe_3O_4@SiO_2@CeO_2	50	92	MB	[28]
Bi_2O_3-Al_2O_3	90	9	MB	[29]
Bi_2O_3-Al_2O_3	90	60	MO	[29]
α-Fe_2O_3	70	97	MB	This work
α-Fe_2O_3	90	91	MO	This work

The kinetic linear curves (Fig. 10) of the photdegradation of MO and MB showed that the degradation followed a simplified Langmuir first-order model, $-\ln(A/A_o) = kt$, at low initial concentration [30]. The rate constants (k) were 0.027 and 0.04 min^{-1} for MO and MB, respectively, confirmed the pseudo first-order reaction [14,15,26,28,30].

The effect of initial concentration of MO and MB dyes on the photocatalyst degradation was investigated, and the degradation profiles are shown in Figs. 9 and 10, respectively. As shown in Figs. 11 and 12, when the initial concentration of dye increased, the speed degradation decreased. These results are similar to the previous works in this area [14].

Photocatalytic activity of the as-prepared α-Fe_2O_3 nanoparticles was notable due to the well crystallinity and the high specific surface area leading to production of the electron-hole pairs [3,14,15,18]. The electron-hole pairs produced the OH° and $O_2^{-\circ}$, and degraded the MO and MB dyes. The possible mechanism of the Photocatalytic degradation of the dyes is presumed to be as following [6,9, 8,24,62]:

$Fe_2O_3 + h\upsilon \rightarrow h^+$ (hole) + e^-

h^+ (hole) + $H_2O \rightarrow H^+ + OH^\circ$

$O_2 + e^- \rightarrow O_2^{-\circ}$

$O_2^{-\circ} + H_2O \rightarrow 2OH^\circ$

$OH^\circ/O_2^{-\circ}$ + MO or MB → degraded products

Finally, the active radicals (OH° and $O_2^{-\circ}$) can damage MO and MB. The oxidation products of the dyes can be deposited on the active surface of the α-Fe_2O_3 nanoparticles. Finally, the stability and reusability of the α-Fe_2O_3 nanoparticles for the photodegradation of MO and MB was studied (Fig. 13). For this matter, the photocatalyst α-Fe_2O_3 was collected after each run, washed using acetone, dried at 150 °C for 3 h, and was used for the photodegradation of MO and MB in the same reaction conditions. As shown in Fig. 13, the efficiency of photocatalytic activity decreased after each recycle [25,28,63,64] due to deactivation the surface of the catalyst [64].

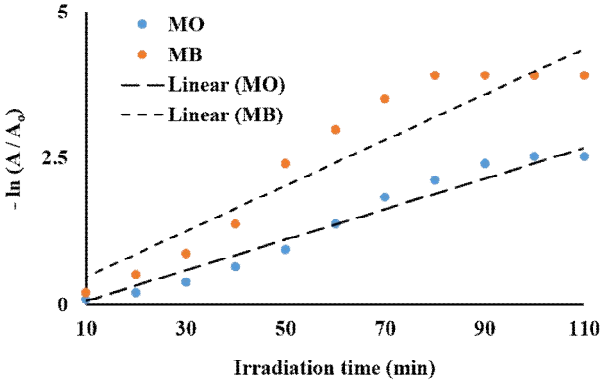

Fig. 10. The pseudo-first order kinetics of MO and MB by the as-prepared α-Fe_2O_3 nanoparticles.

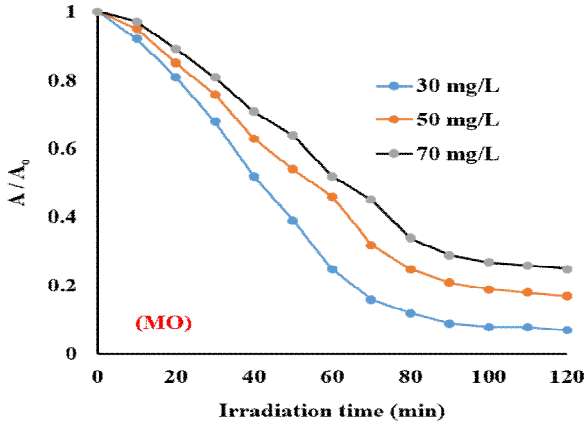

Fig. 11. The effect of initial concentration of MO on degradation efficiency by the as-prepared α-Fe_2O_3 nanoparticles.

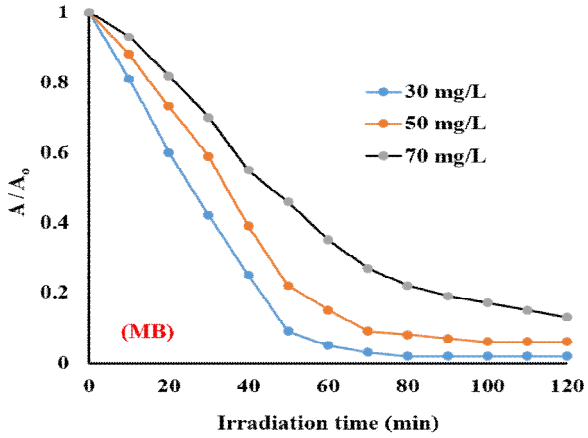

Fig. 12. The effect of initial concentration of MB on degradation efficiency by the as-prepared α-Fe_2O_3 nanoparticles.

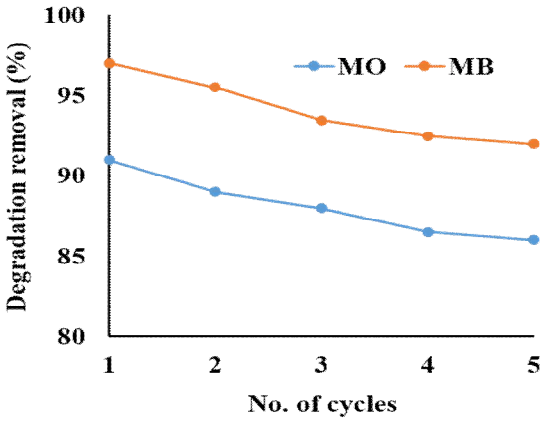

Fig. 13. Reusability studies of the Ce-1 and Ce-2 photocatalyst for 5 recycles runs.

CONCLUSIONS

In summary, α-Fe_2O_3 nanoparticles were successfully synthesized using solid-state thermal decomposition, and characterized by the FT-IR, XRD, VSM, and TEM. FT-IR and XRD results confirmed the preparation of pure rhombohedral phase of α-Fe_2O_3. TEM results showed that the products had quasi-spherical shape with an average crystalline size of 42 nm. VSM result showed the ferromagnetic property of the α-Fe_2O_3 nanoparticles. In addition, photocatalytic degradation reaction of MO and MB dyes confirmed the superior photocatalytic activity of the α-Fe_2O_3. At optimum condition, the maximum degradation removal percentage of the MB and MO were ≈97 and 91%, respectively. The rate constant (k) for MB was higher than that for the MO, due to the better interaction of the positively charged MB with the negatively charged α-Fe_2O_3. Small crystal size, no agglomeration, and high surface area of the as-prepared α-Fe_2O_3 are the key factors that are responsible for the great degradation of the MO and MB dyes. The degradation removal percentage of the as-synthesized α-Fe_2O_3 nanoparticles did not show any obvious decrease after 5 degradation cycles.

ACKNOWLEDGMENTS

The author would like to gratefully acknowledge the Golestan University.

REFERENCES

[1] Xu, J.; Lin, F.; Doeff, M. M.; Tong, W., A review of Ni-based layered oxides for rechargeable Li-ion batteries, *J. Mater. Chem. A* **2017**, *5*, 874-901. DOI: 10.1039/C6TA07991A.

[2] Roy, M.; Ghosh, S.; Naskar, M. K., Synthesis of morphology controllable porous Co_3O_4 nanostructures with tunable textural properties and their catalytic application, *Dalton Trans.* **2014**, *43*, 10248-10257. DOI: 10.1039/C4DT00608A.

[3] Sahu, K.; Singh, J.; Mohapatra, S., Photocatalytic and catalytic removal of toxic pollutants from water using CuO nanosheets, *J. Mater. Sci. Mater. Elect.* **2019**, *30*, 6088-6099. DOI: 10.1007/s10854-019-00910-3.

[4] Zhou, B.; Yang, J.; Jiang, X., Porous Mn_2O_3 nanorods synthesized from thermal decomposition of coordination polymer and used in hydrazine electrochemical sensing, *Mater. Lett.* **2015**, *159*, 362-365. DOI: 10.1016/j.matlet.2015.07.031.

[5] Bai, Z.; Zhang, X.; Zhang, Y.; Guo, C.; Tang, B., Facile synthesis of mesoporous Mn_3O_4 nanorods as a promising anode material for high performance lithium-ion batteries, *J. Mater. Chem. A* **2014**, *2*, 16755-16760. DOI: 1039/C4TA03532A.

[6] Vatanparast, M.; Saedi, L., Sonochemical-assisted synthesis and characterization of CeO_2 nanoparticles and its photocatalytic properties, *J. Mater. Sci.: Mater. Elect.* **2018**, *29*, 7107-7113. DOI: 10.1007/s10854-018-8698-8.

[7] Madkour, M.; Allam, O. G.; Nazeer, A. A.; Amin, M. O.; Al-Hetlani, E., CeO_2-based nanoheterostructures with p-n and n-n heterojunction arrangements for enhancing the solar-driven photodegradation of rhodamine 6G dye, *J. Mater. Sci: Mater. Elect.* **2019**, *30*, 10857-10866. DOI: 10.1007/s10854-019-01429-3.

[8] Lassoued, A.; Lassoued, M. S.; Dkhil, B.; Ammar, S.; Gadri, A., Nanocrystalline NixCo(0.5-x)Zn0.5Fe_2O_4 ferrites: fabrication through co-precipitation route with enhanced structural, magnetic and photocatalytic activity, *J. Mater. Sci: Mater. Elect.* **2018**, *29*, 7333-7344. DOI: 10.1007/s10854-018-8723-y.

[9] Lassoued, A.; Lassoued, M. S.; Dkhil, B.; Ammar, S.; Gadri, A., Photocatalytic degradation of methyl

orange dye by $NiFe_2O_4$ nanoparticles under visible irradiation: effect of varying the synthesis temperature, *J. Mater. Sci: Mater. Elect.* **2018**, *29*, 7057-7067. DOI: 10.1007/s10854-018-8693-0.

[10] Li, Z.; Mao, Y.; Tian, Q.; Zhang, W.; Yang, L., Extremly facile preparation of high-performance Fe_2O_3 anode for lithium-ion batteries, *J. All. Compd.* **2019**, *784*, 125-133. DOI: 10.1016/j.jallcom.2018.12.392.

[11] Jamzad, M.; Bidkopeh, M. K., Green synthesis of iron oxide nanoparticles by the aqueous extract of Laurus nobilis L. leaves and evaluation of the antimicrobial activity, *J. Nanostruct. Chem.* **2020**, *10*, 193-201. DOI: 10.1007/s40097-020-00341-1.

[12] Cao, C. Y.; Qu, J.; Yan, W. S.; Zhu, J. F.; Wu, Z. Y.; Song, W. G., Low-cost synthesis of flowerlike α-Fe_2O_3 nanostrucures for heavy metal ion removal: Adsorption property and mechanism, *Langmuir* **2012**, *28*, 4573-4579. DOI: 10.1021/la300097y.

[13] Dissanayake, D. M. S. N.; Mantilaka, M. M. M. G. P. G.; Palihawadana, T. C.; Chandrakumara, G. T. D.; De Silva, R. T.; Pitawala, H. M. T. G. A.; Nalin de Silva, K. M.; Amaratunga, G. A. J., Facile and low-cost synthesis of pure hematite (α-Fe_2O_3) nanoparticles from naturally occurring laterites and their superior adsorption capability towards acid-dyes, *RSC Adv.* **2019**, *9*, 21249-21257. DOI: 10.1039/C9RA03756J.

[14] Ye, C.; Hu, K.; Niu, Z.; Lu, Y.; Zhang, L.; Yaan, K., Controllable synthesis of rhombohedral α-Fe_2O_3 efficient for photocatalytic degradation of bisphenol A, *J. Water Process Eng.* **2019**, *27*, 205-210. DOI: 10.1016/j.jwpe.2018.12.008.

[15] Gandha, K.; Mohapatra, J.; Hossain, M. K.; Elkins, K.; Poudyal, N.; Rajeshwar, K.; Liu, J. P., Mesoporous iron oxide nanowires: synthesis, magnetic and photocatalytic properties, *RSC Adv.* **2016**, *6*, 90537-90546. DOI: 10.1039/C6RA18530D.

[16] Taghavi Fardood, S.; Moradnia, F.; Moradi, S.; Forootan, R.; Yekke Zare, F.; Heidari, M., Eco-friendly synthesis and characterization of α-Fe_2O_3 nanoparticles and study of their photocatalytic activity for degradation of Congo red dye, *Nanochem. Res.* **2019**, *4*, 140-147. DOI: 10.22036/NCR.2019.02.005.

[17] Kusior, A.; Michalec, K.; Jelen, P.; Radecka, M., Shaped Fe_2O_3 nanoparticles-synthesis and enhanced photocatalytic degradation towards RhB, *App. Surf. Sci.* **2019**, *476*, 342-352. DOI: 10.1016/j.apsusc.2018.12.113.

[18] Wang, J.; Shao, X.; Zhang, Q.; Tian, G.; Ji, X.; Bao, W., Preparation of mesoporous magnetic Fe_2O_3 nanoparticles and its application for organic dye removal, *J. Mol. Liq.* **2017**, *248*, 13-18. DOI: 10.1016/j.molliq.2017.10.026.

[19] Kushwaha, P.; Chauhan, P., Synthesis of spherical and Rod-Like EDTA assisted α-Fe_2O_3 nanoparticles via co-precipitation method, *Mater. Today: Proceed.* **2021**, *44*, 3086-3090. DOI: 10.1016/j.matpr.2021.02.450.

[20] Srivastava, M.; Singh, J.; Yashpal, M.; Ojha, A. K., Synthesis, growth mechanism and characterization of single crystalline α-Fe_2O_3 spherical nanoparticle, *J. Nanosci. Nanotechnol.* **2012**, *12*, 6248-6257. DOI: 10.1166/jnn.2012.6454.

[21] Saghi, M.; Mahanpoor, K.; Shafiei, H., Preparation of nano spherical α-Fe_2O_3 supported on 12-tungstosilicic acid using two different methods: a novel catalyst, *Iran. J. Chem. Chem. Eng.* **2018**, *37*, 1-10. DOI: 10.30492/IJCCE.2018.29140.

[22] Tan, W. F.; Yu, Y. T.; Wang, M. X.; Liu, F.; Koopal, L. K., Shape evolution synthesis of monodisperse spherical, ellipsoidal, and elongated hematite (α-Fe_2O_3) nanoparticles using ascorbic acid, *Cryst. Growth Des.* **2014**, *14*, 157-164. DOI: 10.1021/cg401334d.

[23] Anitha, T.; Senthil Kumar, P.; Sathish Kumar, K., Synthesis of nano-sized chitosan blended polyvinyl alcohol for the removal of eosin yellow dye from aqueous solution, *J. Water Process Eng.* **2016**, *13*, 127-136. DOI: 10.1016/j.jwpe.2016.08.003.

[24] Majumder, D.; Chakraborty, I.; Mandal, K.; Roy, S., Facet-dependent photodegradation of methylene blue using pristine CeO_2 nanostructures, *ACS Omega* **2019**, *4,* 4243-4251. DOI: 10.1021/acsomega.8b03298

[25] Safat, S.; Buazar, F.; Albukhaty, S.; Matroodi, S., Enhanced sunlight photocatalytic activity and biosafety of marine-driven synthesized cerium oxide nanoparticles, *Sci. Rep.* **2021**, *11*, 14734.

DOI: 10.1038/s41598-021-94327-w.

[26] Ynag, X.; Liu, Y.; Li, J.; Zhang, Y., Effects of calcination temperature on morphology and structure of CeO_2 nanofibers and their photocatalytic activity, *Mater. Lett.* **2019**, *241*, 76-79. DOI: 10.1016/j.matlet.2019.01.006.

[27] Snethil Kumar, S.; Lellala, K.; Ashok, M.; Priyadharsan, A.; Sanjeeviraja, S.; Rajendran, A., Green synthesis of CeO_2-TiO_2 compound using Cleome chelidonii leaf extract for excellent photocatalytic activity, *J. Mater. Sci: Mater. Electron.* **2018**, *29*, 14022-14030. DOI: 10.1007/s10854-018-9534-x.

[28] Ziaadini, F.; Mostafavi, A.; Shamspur, T.; Fathirad, F., Photocatalytic degradation of methylene blue from aqueous solution using Fe_3O_4@SiO2@CeO_2 core-shell magnetic nanostructure as an effective catalyst, *Adv. Environment. Technol.* **2019**, *2*, 127-132. DOI: 10.22104/AET.2020.4137.1204.

[29] Hakimi, M.; Morvaridi, M.; Hosseini, H. A.; Alimard. P., Preparation, characterization and photocatalytic activity of Bi_2O_3-Al_2O_3 nanocomposite, *Polyhedron* **2019**, *170*, 523-529. DOI: 10.1016/j.poly.2019.06.029.

[30] Zha, R.; Nadimicherla, R.; Guo, X., Ultraviolet photocatalytic degradation of methyl orange by nanostructured TiO_2/ZnO heterojunctions, *J. Mater. Chem. A* **2015**, *3*, 6565-6574. DOI: 10.1039/c5ta00764j

[31] Akhundi, A.; Badiei, A.; Mohammadi Ziarani, G.; Habibi-Yangjeh, A.; Muñoz-Batista, M. J.; Luque, R., Graphitic carbon nitride-based photocatalysts: Toward efficient organic transformation for value-added chemicals production, *Mol. Catal.* **2020**, *488*, 110902. DOI: 10.1016/j.mcat.2020.110902.

[32] Asadzadeh-Khaneghah, S.; Habibi-Yangjeh, A., g-C_3N_4/carbon dot-based nanocomposites serve as efficacious photocatalysts for environmental purification and energy generation: A review, *J. Cleaner Product.* **2020**, *276*, 124319. DOI: 10.1016/j.jclepro.2020.124319.

[33] Habibi-Yangjeh, A.; Asadzadeh-Khaneghah, S.; Feizpoor, S.; Rouhi, A., Review on heterogeneous photocatalytic disinfection of waterborne, airborne, and foodborne viruses: Can we win against pathogenic viruses? *J. Coll. Interface Sci.* **2020**, *580*, 503-514. DOI: 10.1016/j.jcis.2020.07.047.

[34] Deng, Y.; Zhaio, R., Advanced oxidation processes (AOPs) in wastewater treatment, *Curr. Pollut. Rep.* **2015**, *1*, 167-176. DOI: 10.1007/s40726-015-0015-z.

[35] Audenaert, W. T. M.; Vermeersch, Y.; Van Hulle, S. W. H.; Dejans, P.; Dumouilin, A.; Nopens, I., Application of a mechanistic UV/hydrogen peroxide model at full-scale: Sensitivity analysis, calibration and performance evaluation, *Chem. Eng. J.* **2011**, *171*, 113-126. DOI: 10.1016/j.cej.2011.03.071.

[36] [36] Naddeo, V.; Zarra, T.; Xia, D.; Cai, Y.; Telegin, F.Y.; Pervez, M.N., Efficient Degradation of Mordant Blue 9 Using the Fenton-Activated Persulfate System, *Water.* **2019**, *11*, 2532. DOI: 10.3390/w11122532.

[37] Cai, Q. Q.; Jothinathan, L.; Deng, S. H.; Ong, S. L.; Ng, H. Y.; Hu, J. Y., Shah, M. P., 11- Fenton- and ozone-based AOP processes for industrial effluent treatment, Advanced Oxidation Processes for Effluent Treatment Plants, Elsevier, **2021**, 199-254, DOI: 10.1016/b978-0-12-821011-6.00011-6.

[38] Berberidou, C.; Poulios I.; Xekoukoulotakis, N. P.; Mantzavinos, D., Sonolytic, photocatalytic and sonophotocatalytic degradation of malachite green in aqueous solutions, *App. Catal. B: Environmen.* **2007**, *74*, 63-72.DOI: 10.1016/j.apcatb.2007.01.013.

[39] Aarab, N.; Laabd, M.; Eljazoulo, H.; Lakhmiri, R.; Kabli, H.; Albourine, A., Experimental and DFT studies of the removal of pharmaceutical metronidazole from water using polypyrrole, *Int. J. Indust. Chem.* **2019**, *10*, 269-279. DOI: 10.1007/s40090-019-0190-7.

[40] Palace Carvalho, A. J.; Dordio, A. V.; Prates Ramalho, J. P., A DFT study on the adsorption of benzodiazepines to vermiculite surfaces, *J. Mol. Model.* **2014**, *20*, 2336-. DOI: 10.1007/s00894-014-2336-z.

[41] Jalbani. N. S.; Kaya, S.; Serdaroglu, G.; Şimşek, S.; Memon, S., Experimental and DFT modeling studies for the adsorptive removal of reactive dyes from wastewater, *Sep. Sci. Technol.* **2022**, *57*, 339-353.

DOI: 10.1080/01496395.2021.1900252.

[42] Kitchamsetti, N.; Ramteke, M. S.; Rondiya, S. R.; Mulani, S. R.; Patil, M. S.; Cross, R. W.; Dzade, N. Y.; Devan, R. S., DFT and experimental investigations on the photocatalytic activities of NiO nanobelts for removal of organic pollutants, *J. All. Comd.* **2021**, *855*, 157337. DOI: 10.1016/j.jallcom.2020.157337.

[43] Khalaji, A. D.; Palang Sangdevini, Z.; Mousvi, S. M.; Jarosova, M.; Machek, P., Benzoic acid-functionalized α-Fe_2O_3 nanoparticles: synthesis, characterization, magnetic and optical properties, *Asian J. Nanosci, Mater.* **2020**, *4*, 137-146. DOI: 10.26655/AJNANOMAT.2021.2.4.

[44] Khalaji, A. D.; Ghorbani, M., Thermal studies of iron(II) Schiff base complexes: New precursors for preparation of α-Fe_2O_3 nanoparticles via solid-state thermal decomposition, *Chem. Metod.* **2020**, *4*, 532-542. DOI: 10.33945/SAMI/CHEMM.2020.4.12.

[45] Khalaji, A. D., Synthesis, characterization and optical properties of Co_3O_4 nanoparticles, *Asian J. Nanosci, Mater.* **2019**, *2*, 186-190. DOI: 10.26655/AJNANOMAT.2019.3.5.

[46] Khalaji, A. D.; Ghorbani, M.; Peyghoun, S. J.; Feizi, N.; Akbari, A.; Hornfeck, W.; Dusek, M.; Eigner, V., Vanadium(IV) Schiff base complex: Synthesis, characterization, crystal structure and thermal decomposition of V_2O_5 particles, *Chem. Metod.* **2019**, *3*, 707-714. DOI: 10.33945/SAMI/CHEMM.2019.6.3.

[47] Khalaji, A. D.; Ghorbani, M.; Dusek, M.; Eigner, V., The bis(4-methoxy-2-hydroxybenzophenone) copper(II) complex used as a new precursor for preparation of CuO nanoparticles, *Chem. Metod.* **2020**, *4*, 143-151. DOI: 10.33945/SAMI/CHEMM.2020.2.4.

[48] Zhang, X.; Niu, Y.; Meng, X.; Li, Y.; Zhao, J., Structural evolution and characteristics of the phase transformations between α-Fe_2O_3, Fe_3O_4 and γ-Fe_2O_3 nanoparticles under reducing and oxidizing atmospheres, *Cryst. Eng. Commun.* **2013**, *15*, 8166-8172. DOI: 10.1039/C3CE41269E.

[49] Lassoued, A.; Lassoued, M. S.; Dkhil, B.; Ammar, S.; Gadri, A., Synthesis, photoluminescence and magnetic properties of iron oxide (α-Fe_2O_3) nanoparticles through precipitation or hydrothermal methods, *Phys. E.* **2018**, *101*, 212-219. DOI: 10.1016/j.physe.2018.04.009.

[50] Liu, J.; Yang, H.; Xue, X., Preparation of different shaped α-Fe_2O_3 nanoparticles with large particle of iron oxide red, *CryetEngComm.* **2019**, *21*, 1097-1101. DOI: 10.1039/C8CE01920G.

[51] Han, C.; Han, J.; Li, Q.; Xie, J., Wet chemical controllable synthesis of hematite ellipsoids with structurally enhanced visible light property, *Sci. World J.* **2013**, Article ID 410594, 5 pages. DOI: 10.1155/2013/410594.

[52] Khalaji, A. D.; Mousavi, S. M.; Palang Sangdevini, Z.; Jarosova, M.; Machek, P.; Dusek, M., Hematite (α-Fe_2O_3) nanoparticles: synthesis, characterization and optical properties , *J. Sci: IRI.* **2021**, *32*, 213-219. DOI: 10.22059/JSCIENCES.2021.312076.1007584.

[53] Negi, K.; Kumar, M.; Singh, G.; Chauhan, S.; Chauhan, M. S., Nanostructured CeO_2 for selective-sensing and smart photocatalytic applications, *Cer. Int.* **2018**, *44*, 15281-15289. DOI: 10.1016/j.ceramint,2018.05.172

[54] Nawi, M. A.; Sabar, S., Photocatalytic decolourisation of Reactive Red 4 dye by an immobilised TiO_2/chitosan layer by layer system, *J. Coll. Interface Sci.* **2012**, *372*, 80-87. DOI: 10.1016/j.jcis.2012.01.024.

[55] Shahrezaei, F.; Mansouri, Y.; Zinatizadeh, A. A. L.; Akhbari, A., Process modeling and kinetic evaluation of petroleum refinery wastewater treatment in a photocatalytic reactor using TiO_2 nanoparticles, *Powder Technol.* **2012**, *221*, 203-212. DOI: 10.1016/j.powtec.2012.01.003.

[56] Pelaez, M.; de la Cruz, A. A.; O'Shea, K.; Falaras, P.; Dionysiou, D. D., Effects of water parameters on the degradation of microcystin-LR under visible light-activated TiO_2 photocatalyst, *Water Res.* **2011**, *45*, 3787-3796. DOI: 10.1016/j.watres.2011.04.036.

[57] Song, S.; Xu, L.; He, Z., Photocatalytic degradation of C.I. Direct Red 23 in aqueous solutions under UV irradiation using $SrTiO_3$/CeO_2 composite as the catalyst, *J. Hazard. Mater.* **2008**, *152*, 1301-1308. DOI: 10.1016/j.jhazmat.2007.08.004.

[58] Chen, S. F.; Liu, Y. Z., Study on the photocatalytic

degradation of glyphosate by TiO_2 photocatalyst, *Chemosphere* **2007**, *67*, 1010-1017. DOI: 10.1016/j.chemosphere.2006.10.054.

[59] Mahmoodi, N. M.; Arami, M.; Zhang, J., Preparation and photocatalytic activity of immobilized composite photocatalyst (titania nanoparticle/activated carbon), *J. All. Compd*. **2011**, *509*, 4754-4764. DOI: 10.1016/j.jallcom.2011.01.146.

[60] Caliman, A. F.; Cojocaru, C.; Antoniadis, A.; Poulios, I., Optimized photocatalytic degradation of Alcian Blue 8 GX in the presence of TiO_2 suspensions, *J. Hazard. Mater*. **2007**, *144*, 265-273. DOI: 10.1016/j.jhazmat.2006.10.019.

[61] Szeto, W.; Kan, C. W.; Yuen, C. W. M.; Chan, S. W.; Lam, K. H., Effective photodegradation of methyl orange using fluidized bed reactor loaded with cross-linked chitosan embedded nano-CdS photocatalyst, *Int. J. Chem. Eng*. **2014**, Article ID 270946, 16 pages. DOI: 10.1155/2014/270946.

[62] Ma, R.; Zhang, S.; Wen, T.; Gu, P.; Li, L.; Zhao, G.; Niu, F.; Huang, Q.; Tang, Z.; Wang, X., A critical review on visible-light-response CeO_2-based photocatalysts with enhanced photooxidation of organic pollutants, *Cat. Today* **2019**, *335*, 20-30. DOI: 10.1016/j.cattod.2018.11.016.

[63] Malleshappa, J.; Nagabhushana, H.; Sharma, S. C.; Vidya, Y. S.; Anantharaju, K. S.; Prashantha, S. C.; Daruka Prasad, B.; Raja Naika, H.; Lingaraju, K.; Surendra, B. S., Leucas aspera mediated multifunctional CeO_2 nanoparticles: Structural, photoluminescent, photocatalytic and antibacterial properties, *Spectrochim. Acta A* **2015**, *149*, 452-462.

[64] Kunjachan, C.; Kurian, M., Cerium oxide-based nanostructures as efficient catalysts for transesterification of mthylacetate with n-butanol, *Clean. Eng. Technol.* **2021**, *4*, 100232. DOI: 10.1016/j.clet.2021.100232.